

# Time-reversal symmetry breaking in Re-based superconductors

T. Shang,<sup>1,2,3,\*</sup> M. Smidman,<sup>4,†</sup> S. K. Ghosh,<sup>5</sup> C. Baines,<sup>6</sup> L. J. Chang,<sup>7</sup> D. J. Gawryluk,<sup>1</sup>  
J. A. T. Barker,<sup>6</sup> R. P. Singh,<sup>8</sup> D. McK. Paul,<sup>9</sup> G. Balakrishnan,<sup>9</sup> E. Pomjakushina,<sup>1</sup> M. Shi,<sup>2</sup>  
M. Medarde,<sup>1</sup> A. D. Hillier,<sup>10</sup> H. Q. Yuan,<sup>4,11</sup> J. Quintanilla,<sup>5,‡</sup> J. Mesot,<sup>12,3,13</sup> and T. Shiroka<sup>13,12,§</sup>

<sup>1</sup>Laboratory for Multiscale Materials Experiments, Paul Scherrer Institut, Villigen CH-5232, Switzerland

<sup>2</sup>Swiss Light Source, Paul Scherrer Institut, Villigen CH-5232, Switzerland

<sup>3</sup>Institute of Condensed Matter Physics, École Polytechnique Fédérale de Lausanne (EPFL), Lausanne CH-1015, Switzerland.

<sup>4</sup>Center for Correlated Matter and Department of Physics, Zhejiang University, Hangzhou 310058, China

<sup>5</sup>School of Physical Sciences, University of Kent, Canterbury CT2 7NH, United Kingdom

<sup>6</sup>Laboratory for Muon-Spin Spectroscopy, Paul Scherrer Institut, CH-5232 Villigen PSI, Switzerland

<sup>7</sup>Department of Physics, National Cheng Kung University, Tainan 70101, Taiwan

<sup>8</sup>Indian Institute of Science Education and Research Bhopal, Bhopal, 462066, India

<sup>9</sup>Physics Department, University of Warwick, Coventry CV4 7AL, United Kingdom

<sup>10</sup>ISIS Facility, STFC Rutherford Appleton Laboratory, Harwell Science and Innovation Campus, Oxfordshire, OX11 0QX, United Kingdom

<sup>11</sup>Collaborative Innovation Center of Advanced Microstructures, Nanjing University, Nanjing 210093, China

<sup>12</sup>Paul Scherrer Institut, CH-5232 Villigen PSI, Switzerland

<sup>13</sup>Laboratorium für Festkörperphysik, ETH Zürich, CH-8093 Zurich, Switzerland

To trace the origin of time-reversal symmetry breaking (TRSB) in Re-based superconductors, we performed comparative muon-spin rotation/relaxation ( $\mu$ SR) studies of superconducting noncentrosymmetric  $\text{Re}_{0.82}\text{Nb}_{0.18}$  ( $T_c = 8.8$  K) and centrosymmetric Re ( $T_c = 2.7$  K). In  $\text{Re}_{0.82}\text{Nb}_{0.18}$ , the low-temperature superfluid density and the electronic specific heat evidence a fully-gapped superconducting state, whose enhanced gap magnitude and specific-heat discontinuity suggest a moderately strong electron-phonon coupling. In both  $\text{Re}_{0.82}\text{Nb}_{0.18}$  and pure Re, the spontaneous magnetic fields revealed by zero-field  $\mu$ SR below  $T_c$  indicate time-reversal symmetry breaking and thus unconventional superconductivity. The concomitant occurrence of TRSB in centrosymmetric Re and noncentrosymmetric ReT ( $T$  = transition metal), yet its preservation in the isostructural noncentrosymmetric superconductors  $\text{Mg}_{10}\text{Ir}_{19}\text{B}_{16}$  and  $\text{Nb}_{0.5}\text{Os}_{0.5}$ , strongly suggests that the local electronic structure of Re is crucial for understanding the TRSB superconducting state in Re and ReT. We discuss the superconducting order parameter symmetries that are compatible with the observations.

Time reversal and spatial inversion are two key symmetries which influence at a fundamental level the electron pairing in the superconducting state: on the one hand, a number of unconventional superconductors exhibit spontaneous time-reversal symmetry breaking (TRSB) on entering the superconducting state; on the other hand, the absence of inversion symmetry above  $T_c$  leads to an anti-symmetric spin-orbit coupling (SOC), lifting the degeneracy of the conduction-band electrons and potentially giving rise to a mixed-parity superconducting state [1, 2]. Some noncentrosymmetric superconductors (NCSC), such as  $\text{CePt}_3\text{Si}$  [3],  $\text{CeIrSi}_3$  [4],  $\text{Li}_2\text{Pt}_3\text{B}$  [5, 6], and  $\text{K}_2\text{Cr}_3\text{As}_3$  [7, 8], exhibit line nodes in the gap, while others such as  $\text{LaNiC}_2$  [9] and  $(\text{La,Y})_2\text{C}_3$  [10], show multiple nodeless superconducting gaps. In addition, due to the strong influence of SOC, their upper critical field can greatly exceed the Pauli limit, as has been found in  $\text{CePt}_3\text{Si}$  [11] and very recently in  $(\text{Ta,Nb})\text{Rh}_2\text{B}_2$  [12].

In general, TRSB below  $T_c$  and a lack of spatial-inversion symmetry of the crystal structure are independent events. Yet, in a few cases, such as in  $\text{LaNiC}_2$  [13],  $\text{La}_7\text{Ir}_3$  [14], and, in particular, in the Re-based compounds  $\text{Re}_6\text{Zr}$  [15],  $\text{Re}_6\text{Hf}$  [16],  $\text{Re}_6\text{Ti}$  [17], and  $\text{Re}_{24}\text{Ti}_5$  [18], TRSB below  $T_c$  is concomitant with an existing lack of crystal inversion symmetry. Such an unusually frequent occurrence of TRSB among the superconducting ReT binary alloys ( $T$  = transition metal) is rather puzzling. Its persistence independent of the particular transition metal, points to a key role played by Re. To test such a hypothesis, and to ascertain the possible relevance of the noncentrosymmetric structure to TRSB in Re-based NCSC, we proceeded with a twofold study. On one hand we synthesized and investigated an-

other Re-based NCSC,  $\text{Re}_{0.82}\text{Nb}_{0.18}$ . On the other hand, we considered the pure Re metal, also a superconductor, but with a centrosymmetric structure.

A comparative study by means of muon-spin relaxation and rotation ( $\mu$ SR) allows us to address the question of TRSB in Re-containing compounds. The choice of  $\mu$ SR as the preferred technique for our study is justified by its key role in detecting TRSB in numerous unconventional superconductors [13–20] (later confirmed by Kerr effect or bulk magnetisation in the cases of  $\text{Sr}_2\text{RuO}_4$ ,  $\text{UPt}_3$  and  $\text{LaNiC}_2$  [21–23]). We report systematic  $\mu$ SR studies of  $\text{Re}_{0.82}\text{Nb}_{0.18}$  ( $T_c = 8.8$  K) and Re ( $T_c = 2.7$  K), whose bulk superconducting properties were characterized by magnetic, transport, and thermodynamic measurements. The  $\mu$ SR data show that spontaneous magnetic fields appear below the respective transition temperatures, thus implying that the superconducting states of both  $\text{Re}_{0.82}\text{Nb}_{0.18}$  and Re show TRSB and have an unconventional nature. Since pure Re is centrosymmetric, this implies that the noncentrosymmetric structure is not a requirement for TRSB in these materials.

Polycrystalline  $\text{Re}_{0.82}\text{Nb}_{0.18}$  samples were prepared by arc melting Re and Nb metals and the same Re powder was used for measurements on elementary Re. The x-ray powder diffraction measured using a Bruker D8 diffractometer, confirmed the  $\alpha$ -Mn structure of  $\text{Re}_{0.82}\text{Nb}_{0.18}$  ( $I43m$ ) and the hcp-Mg structure of Re ( $P6_3/mmc$ ) [24–30]. Magnetic susceptibility, electrical resistivity, and specific-heat measurements were performed on a 7-T Quantum Design Magnetic Property Measurement System and a 9-T Physical Property Measurement System. The  $\mu$ SR measurements were carried out on both the  $\mu$ SR instrument of the ISIS pulsed

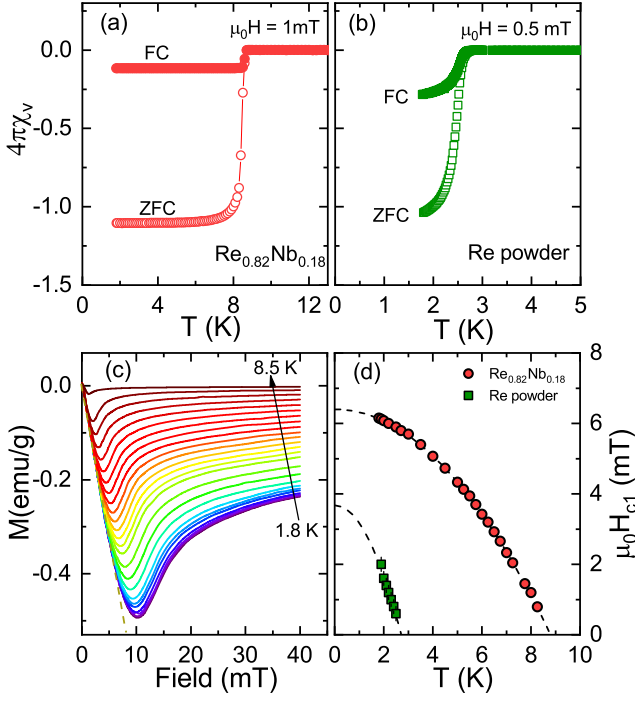


FIG. 1. Temperature-dependent magnetic susceptibilities of (a)  $\text{Re}_{0.82}\text{Nb}_{0.18}$ , and (b) pure Re, measured at 1 mT and 0.5 mT, respectively. (c) Magnetization vs. applied magnetic field recorded at different temperatures up to  $T_c$  for  $\text{Re}_{0.82}\text{Nb}_{0.18}$ . For each temperature,  $\mu_0 H_{c1}$  was determined from the value where  $M(H)$  deviates from linearity (see dashed line). (d)  $\mu_0 H_{c1}$  vs. temperature for both samples; dashed lines represent fits to  $\mu_0 H_{c1}(T) = \mu_0 H_{c1}(0)[1 - (T/T_c)^2]$ .

muon source (UK) [31], and the GPS and LTF spectrometers of the  $\pi\text{M3}$  beamline at the Paul Scherrer Institut, Villigen, Switzerland.

The magnetic susceptibility was determined using both field-cooled (FC) and zero-field-cooled (ZFC) protocols. As shown in Fig. 1(a)-(b), the splitting of the two curves is typical of type-II superconductors, with the ZFC-susceptibility indicating bulk superconductivity with  $T_c = 8.8\text{ K}$  for  $\text{Re}_{0.82}\text{Nb}_{0.18}$  and  $2.7\text{ K}$  for Re. The bulk superconductivity of  $\text{Re}_{0.82}\text{Nb}_{0.18}$  was further confirmed by electrical resistivity and specific-heat data [24]. To perform transverse-field muon-spin rotation (TF- $\mu\text{SR}$ ) measurements of superconductors, the applied field should exceed the lower critical field  $\mu_0 H_{c1}$ , so that the additional field-distribution broadening due to the flux-line lattice (FLL) can be determined from the depolarization of the  $\mu\text{SR}$  asymmetry. To determine  $\mu_0 H_{c1}$ , the field-dependent magnetization  $M(H)$  was measured at various temperatures below  $T_c$ , as shown in Fig. 1(c) for  $\text{Re}_{0.82}\text{Nb}_{0.18}$  [for  $M(H)$  data of Re see Suppl. Mater.] [24]. The derived  $\mu_0 H_{c1}$  values are plotted in Fig. 1(d) as a function of temperature. The dashed lines are fits to  $\mu_0 H_{c1}(T) = \mu_0 H_{c1}(0)[1 - (T/T_c)^2]$ , which yield estimates of lower critical fields of  $6.4(1)\text{ mT}$  and  $3.7(2)\text{ mT}$  in  $\text{Re}_{0.82}\text{Nb}_{0.18}$  and Re, respectively.

The TF- $\mu\text{SR}$  measurements allowed us to explore the nature of superconductivity in  $\text{Re}_{0.82}\text{Nb}_{0.18}$  at a microscopic level. The optimal field value for such experiments (above  $H_{c1}$ ) was determined via preliminary field-dependent  $\mu\text{SR}$  measurements at  $1.5\text{ K}$  [24]. Figure 2(a) shows two rep-

resentative TF- $\mu\text{SR}$  spectra collected above and below  $T_c$  in an applied field of  $15\text{ mT}$ . In the superconducting mixed state, the faster decay of muon-spin polarization reflects the inhomogeneous field distribution due to the FLL. The corresponding TF spectra are described by:

$$P_{\text{TF}} = P_s \cos(\gamma_\mu B_s t + \phi) e^{-\sigma^2 t^2/2} + P_{\text{bg}} \cos(\gamma_\mu B_{\text{bg}} t + \phi).$$

Here  $P_s$  and  $P_{\text{bg}}$  represent the muon-spin polarization for muons implanted in the sample and sample holder, respectively, with the latter not undergoing any depolarization.  $\gamma_\mu = 2\pi \times 135.53\text{ MHz/T}$  is the muon gyromagnetic ratio,  $B_s$  and  $B_{\text{bg}}$  are the respective local fields sensed by implanted muons in the sample and sample holder,  $\phi$  is the initial phase, and  $\sigma$  is a Gaussian relaxation rate. In the superconducting state, the Gaussian relaxation rate includes contributions from both the FLL ( $\sigma_{\text{sc}}$ ) and a temperature-independent relaxation due to nuclear moments ( $\sigma_n$ ). Below  $T_c$ ,  $\sigma_{\text{sc}}$  can be extracted after subtracting  $\sigma_n$  in quadrature, i.e.,  $\sigma_{\text{sc}} = \sqrt{\sigma^2 - \sigma_n^2}$ . Since  $\sigma_{\text{sc}}$  is directly related to the magnetic penetration depth and hence the superfluid density, the superconducting gap value and its symmetry can be determined from the measured relaxation rate.

As shown in the inset of Fig. 2(b), a clear diamagnetic shift appears below  $T_c$ . At the same temperature, the formation of the FLL is apparent from the rapid increase of  $\sigma_{\text{sc}}$ , in turn reflecting an increase of the superfluid density. For small applied magnetic fields [ $H_{\text{appl}}/H_{c2} \ll 1$ ], the effective penetration depth  $\lambda_{\text{eff}}$  can be calculated from [32, 33]:

$$\frac{\sigma_{\text{sc}}^2(T)}{\gamma_\mu^2} = 0.00371 \frac{\Phi_0^2}{\lambda_{\text{eff}}^4(T)}. \quad (1)$$

Figure 2(b) shows the normalized superfluid density  $[\lambda(T)/\lambda(0)]^{-2}$  vs. the reduced temperature  $T/T_c$  for  $\text{Re}_{0.82}\text{Nb}_{0.18}$ . Clearly the temperature dependence of the superfluid density is highly consistent between PSI and ISIS, and well described by an  $s$ -wave model with a single gap of  $1.61(1)\text{ meV}$ . By using the  $15\text{-mT}$  data, the resulting  $\lambda(0)$  of  $357(3)\text{ nm}$  is comparable with  $352(3)\text{ nm}$ , the value calculated from  $\mu_0 H_{c1}$  [24]. The superconducting gap is similar to that of other ReT superconductors, e.g.,  $\text{Re}_6\text{Zr}$  ( $1.21\text{ meV}$ ) [15, 34],  $\text{Re}_{24}\text{Ti}_5$  ( $1.08\text{ meV}$ ) [18],  $\text{Re}_6\text{Ti}$  ( $0.95\text{ meV}$ ) [17], and  $\text{Re}_6\text{Hf}$  ( $1.10\text{ meV}$ ) [16, 35, 36], (see also Table SI in Suppl. Mater.) [24]. Also the  $2\Delta/k_B T_c$  values of these compounds [e.g.,  $4.26$  for  $\text{Re}_{0.82}\text{Nb}_{0.18}$ ] are higher than  $3.53$ , the value expected for weakly-coupled BCS superconductors, thus indicating a moderately strong electron-phonon coupling in these materials. The superconducting parameters of all these  $\alpha$ -Mn-type ReT NCSC are summarized in Table SI in Suppl. Mater. [24].

A detailed analysis of the zero-field specific-heat data provides further insight into the superconducting properties of  $\text{Re}_{0.82}\text{Nb}_{0.18}$ . The electronic specific heat  $C_e/T$  was obtained by subtracting the phonon contribution from the experimental data [24]. The derived  $C_e/T$  was then divided by the normal-state electronic specific heat coefficient, as shown in the main panel as a function of  $T/T_c$ . The solid line in Fig. 2(c) represents a fit with  $\gamma_n = 4.4\text{ mJ mol}^{-1}\text{ K}^{-2}$  and a single isotropic gap  $\Delta(0) = 1.52(2)\text{ meV}$ . This reproduces very well the experimental data, while being consistent with the TF- $\mu\text{SR}$  [see Fig. 2(b)] and previously reported

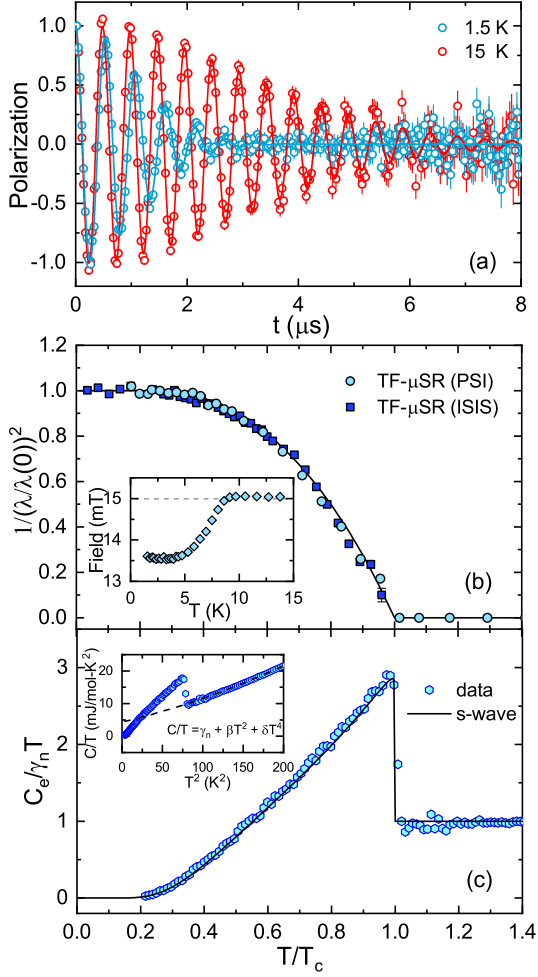


FIG. 2. (a) Time-domain TF- $\mu$ SR spectra in the superconducting and normal states of  $\text{Re}_{0.82}\text{Nb}_{0.18}$ , which show very different relaxation rates. (b) Normalized superfluid density vs. temperature, as determined from  $\mu$ SR measurements. Inset: temperature dependence of the internal field across  $T_c$ . (c) Temperature dependence of the zero-field electronic specific heat. The inset shows the total  $C/T$  data versus  $T^2$ . The dashed-line is a fit to  $C/T = \gamma_n + \beta T^2 + \delta T^4$ , used to estimate the phonon contribution. The solid lines in (b) and (c) represent fits using a fully-gapped  $s$ -wave model.

values [37, 38]. We also note this value is between the two values found from a two-gap analysis [39]. The specific-heat jump at  $T_c$  was found to be  $\Delta C/\gamma_n T_c \sim 1.94$ , i.e., larger than the conventional BCS value of 1.43, again indicating a moderately enhanced electron-phonon coupling in  $\text{Re}_{0.82}\text{Nb}_{0.18}$ .

The key goal of the present work is to probe a possible TRSB in  $\text{Re}_{0.82}\text{Nb}_{0.18}$  and in pure Re. To this aim we performed detailed zero-field muon-spin relaxation (ZF- $\mu$ SR) measurements. Normally, in the absence of external fields, the onset of superconductivity does not imply changes in the ZF muon-spin relaxation rate. However, in presence of TRSB, the onset of a tiny spontaneous polarization or currents gives rise to associated (weak) magnetic fields, readily detected by ZF- $\mu$ SR as an increase in muon-spin relaxation rate. Given the tiny size of such effects, we measured the ZF- $\mu$ SR both above  $T_c$  and inside the superconducting phase. Representative ZF- $\mu$ SR spectra collected above and below  $T_c$  for  $\text{Re}_{0.82}\text{Nb}_{0.18}$  and Re show measurable differences [see Fig. 3(a)-(b)]. To exclude the presence of stray

magnetic fields, all magnets were quenched before the measurements and an active compensation system was used. In non-magnetic materials in the absence of applied fields, the relaxation is determined primarily by the randomly oriented nuclear dipole moments, normally described by a Gaussian Kubo-Toyabe relaxation function [40, 41]. In our case, the ZF- $\mu$ SR spectra are well described by a combined Lorentzian and Gaussian Kubo-Toyabe relaxation function:

$$P_{\text{CKT}} = P_s \left[ \frac{1}{3} + \frac{2}{3}(1 - \sigma^2 t^2 - \Lambda t) e^{\left(-\frac{\sigma^2 t^2}{2} - \Lambda t\right)} \right] + P_{\text{bg}}. \quad (2)$$

Here  $P_s$  and  $P_{\text{bg}}$  are the same as in the TF- $\mu$ SR spectra. As shown in the insets of Fig. 3, despite the different  $T_c$  values of  $\text{Re}_{0.82}\text{Nb}_{0.18}$  and Re, their  $\sigma(T)$  curves exhibit a small yet *distinct increase* below  $T_c$ , similar to that found also in other ReT NCSC [15–18]. At the same time, the Lorentzian relaxation rate  $\Lambda(T)$  remains mostly constant in the studied temperature range, with typical values of 0.007 and 0.005  $\mu\text{s}^{-1}$  for  $\text{Re}_{0.82}\text{Nb}_{0.18}$  and Re [24], respectively, indicating that fast-fluctuation effects are absent in these systems. The small, yet measurable increases of  $\sigma(T)$  below  $T_c$ , detected from measurements at both facilities, reflect the onset of spontaneous magnetic fields and thus are signatures of TRSB in the superconducting phases of both  $\text{Re}_{0.82}\text{Nb}_{0.18}$  and Re. Further refinements performed by fixing the  $\Lambda$  values gave similarly robust features in  $\sigma(T)$  [24]. To rule out the possibility of a defect-/impurity-induced relaxation at low temperatures, we performed auxiliary longitudinal-field  $\mu$ SR measurements at 1.5 K. As shown in Figs. 3(a)-(b), a small field of 15 mT is sufficient to decouple the muon spins from the weak spontaneous magnetic fields in both samples, indicating that the relevant fields are static on the time scale of the muon lifetime.

To date, most  $\alpha$ -Mn-type ReT-NCSC have been found to exhibit TRSB in the superconducting state [15–18]. Our results show that  $\text{Re}_{0.82}\text{Nb}_{0.18}$  is not just another member of the ReT-NCSC family, but one with the most distinct TRSB in the superconducting state (i.e., with the highest  $\sigma_{\text{int}}$ , which represents the change of muon relaxation rate between the normal and superconducting states (see details in Table SI in Suppl. Mater.) [24]. This is clearly depicted in Fig. 3(c), where we plot the estimated internal field  $B_{\text{int}}$  as a function of the nuclear magnetic moment  $\mu_n$  for the ReT-NCSC. It can be seen that,  $B_{\text{int}} (\propto \sigma_{\text{int}})$  scales linearly with  $\mu_n$ , reaching 0.038 mT for  $\text{Re}_{0.82}\text{Nb}_{0.18}$ . At the other extreme, the line crosses the horizontal axis at  $\mu_n \sim 2.7\mu_n$ , where  $\sigma_{\text{int}}$  drops below the resolution of the  $\mu$ SR technique (0.01 mT). This is exactly the case for  $\text{Re}_3\text{W}$ , whose  $\sigma_{\text{int}}$  turned out to be negligible [42].

Having detected TRSB in Re-based superconductors still leaves open the most intriguing question: what is its key ingredient? In ReT, the replacement of heavy 5d elements, such as Hf, with lighter 3d elements, such as Ti, appears to have a negligible effect on TRSB. The insensitivity of TRSB to the specific transition-metal element  $T$  suggests that a substitution at the  $T$ -sites does not significantly influence it. This is confirmed by the persistence of TRSB in elemental Re. In addition, this indicates also that a lack of inversion symmetry is inessential. Finally, there is no TRSB in the superconducting states of  $\text{Mg}_{10}\text{Ir}_{19}\text{B}_{16}$  [43] and  $\text{Nb}_{0.5}\text{Os}_{0.5}$  [44], two NCSCs isostructural to ReT and with similar SOC strengths. The above considerations strongly



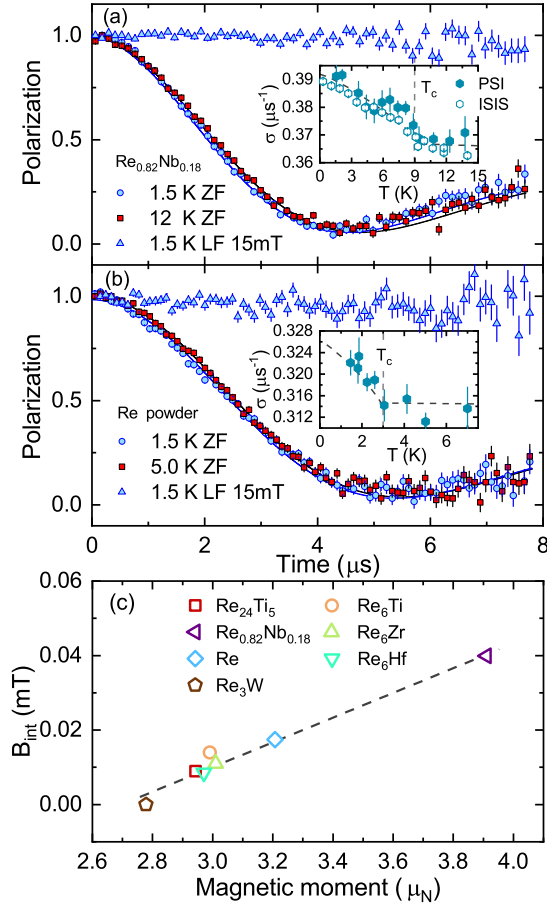


FIG. 3. Representative zero-field  $\mu\text{SR}$  spectra for (a)  $\text{Re}_{0.82}\text{Nb}_{0.18}$  and (b) pure Re metal in the superconducting and normal states. Additional  $\mu\text{SR}$  data sets collected at 1.5 K in a 15-mT longitudinal field, are also shown. The solid lines are fits using Eq. (2). Insets show the  $T$ -dependence of the relaxation rate  $\sigma$ . The results from ISIS in (a) were obtained by fitting the ZF data with the corresponding expression in Ref. 15. (c) Calculated internal field vs. nuclear magnetic moment for ReT superconductors. For the pure Re (diamond), the value was obtained by an extrapolation to 0 K. The reported data are from Refs. 15–18, 34–36, and 42. The dashed-line indicates a linear behavior. The nuclear moment was estimated from the respective nuclear moments  $\mu_{n,\text{Re}}$ ,  $\mu_{n,\text{T}}$  and chemical fractions  $f_{\text{Re}}$  and  $f_{\text{T}}$  of Re and T using  $\mu_n = \sqrt{f_{\text{Re}}\mu_{n,\text{Re}}^2 + f_{\text{T}}\mu_{n,\text{T}}^2}$ .

suggest that it is the *local electronic structure* of Re that is crucial for understanding the TRSB in the superconducting states of Re and ReT. To reinforce the above conclusion, one could study other Re-free materials with the  $\alpha$ -Mn-type structure. TaOs, with a bulk  $T_c$  of 2.07 K and the required crystal structure, represents a good example [45].

We now discuss the possible symmetries of the superconducting order parameter. In the limit of weak SOC, TRSB can be achieved *via* nonunitary triplet pairing, as e.g., in  $\text{LaNiC}_2$  [46] and  $\text{LaNiGa}_2$  [47, 48]. More generally, the relationship between TRSB and triplet pairing is quite complex. For example, the admixed triplet component in so-called ‘s-wave’ NCSC (those whose superconducting instabilities do not break crystal point-group symmetries), such as  $\text{Li}_2\text{Pt}_3\text{B}$ , does not show TRSB [5]. Conversely, there are TRSB states not involving triplet pairing, e.g., the  $s + id$  singlet state proposed for some iron-based superconductors [49]. Apart from the weak-SOC nonunitary triplet pairing scenario mentioned above [46, 47], the essential requirement for TRSB

occurrence is that the point group of the crystal has irreducible representations (irreps) with dimension  $D > 1$ .

The point groups  $T_d$  and  $D_{6h}$  relevant to ReT and Re, respectively, have several irreps with  $D = 2$  or 3. Therefore, they can support TRSB states with singlet-, triplet-, or, in the case of ReT, admixed pairing, independent of SOC strength. In what follows, we will assume strong SOC. The full symmetry analysis and plots of the possible order parameters can be found in the Suppl. Mat. [24]. For ReT there are a number of possible TRSB states, with some examples of pairing functions being given in Ref. 15. However, all the possible states have symmetry-constrained point or line nodes, inconsistent with the experimental observations. In view of this, in some systems, it has been proposed that a full gap may be obtained through a Loop-Josephson-Current (LJC) state built on on-site, intra-orbital, singlet pairing. Although it has been shown that the crystal symmetry of ReT is compatible with this scenario [50], the energetics which would drive such a state, if realized, and why it would occur only in systems with Re and not other elements, remain unclear.

The symmetry analysis of pure Re contrasts strongly that of ReT. Firstly, Re is centrosymmetric, implying that the superconducting instability can only take place in either purely-singlet or purely-triplet channels (irrespective of the strength of SOC). Secondly, due to only two distinct symmetry-related sites per unit cell, a LJC state here is not the most natural one [50]. Thirdly, the crystallographic space group is nonsymmorphic, which in principle allows superconducting instabilities that break screw-axis or glide-plane symmetries. Ignoring the ones that break those symmetries, we find two possible TRSB states, one in the singlet channel with a line node at  $k_z = 0$ , and another in the triplet channel, with two point nodes on the  $k_z$  axis (see Suppl. Mater. [24]). The Fermi surface of Re has five sheets, including an electron sheet centered on the  $\Gamma$  point and open along the  $k_z$  axis and three hole sheets which are closed, centered on the  $L$  point, and not intersecting the  $k_z = 0$  plane [51]. These would be compatible with a full gap for the triplet and singlet TRSB states, respectively.

In summary, we performed comparative  $\mu\text{SR}$  studies of the noncentrosymmetric  $\text{Re}_{0.82}\text{Nb}_{0.18}$  and centrosymmetric Re superconductors. Bulk superconductivity with  $T_c = 8.8$  K ( $\text{Re}_{0.82}\text{Nb}_{0.18}$ ) and 2.7 K (Re) was characterized by magnetic and transport properties. Both the superfluid density and the zero-field specific-heat data reveal a single-gap nodeless superconductivity in  $\text{Re}_{0.82}\text{Nb}_{0.18}$ . The spontaneous fields appearing below  $T_c$ , which increase with decreasing temperature, provide strong evidence that the superconducting states of both noncentrosymmetric  $\text{Re}_{0.82}\text{Nb}_{0.18}$  and centrosymmetric Re show TRSB and are unconventional. Comparisons with other Re-free  $\alpha$ -Mn-type superconductors suggest that in the ReT family, the TRSB is crucially related to the presence of Re, a key idea for understanding the peculiar behavior of ReT superconductors. We have considered the possible symmetries of the order parameter in these systems and their compatibility with the observed fully-gapped spectrum. Further theoretical and experimental work on Re is required to clarify the open issues.

**Acknowledgments:** This work was supported by the National Key R&D Program of China (Grants No. 2017YFA-

0303100 and 2016YFA0300202), the Natural Science Foundation of China (Grant No. 11474251), and the Schweizerische Nationalfonds zur Förderung der Wissenschaftlichen Forschung (SNF). The work at the University of Warwick was supported by EPSRC UK through Grant EP/M028771/1. Experiments at the ISIS Pulsed Neutron and Muon Source were supported by a beamtime allocation from STFC. SKG and JQ are supported by EPSRC through the project “Unconventional Superconductors: New paradigms for new materials” (grant references EP/P00749X/1 and EP/P007392/1).

\* Corresponding authors:

[tian.shang@psi.ch](mailto:tian.shang@psi.ch)

† Corresponding authors:

[mmsmidman@zju.edu.cn](mailto:mmsmidman@zju.edu.cn)

‡ Corresponding authors:

[j.quintanilla@kent.ac.uk](mailto:j.quintanilla@kent.ac.uk)

§ Corresponding authors:

[tshiroka@phys.ethz.ch](mailto:tshiroka@phys.ethz.ch)

- [1] E. Bauer and M. Sigrist, eds., *Non-Centrosymmetric Superconductors*, Vol. 847 (Springer Verlag, Berlin, 2012).
- [2] M. Smidman, M. B. Salamon, H. Q. Yuan, and D. F. Agterberg, *Rep. Prog. Phys.* **80**, 036501 (2017).
- [3] I. Bonalde, W. Brämer-Escamilla, and E. Bauer, *Phys. Rev. Lett.* **94**, 207002 (2005).
- [4] H. Mukuda, T. Fujii, T. Ohara, A. Harada, M. Yashima, Y. Kitaoka, Y. Okuda, R. Settai, and Y. Onuki, *Phys. Rev. Lett.* **100**, 107003 (2008).
- [5] H. Q. Yuan, D. F. Agterberg, N. Hayashi, P. Badica, D. Vandervelde, K. Togano, M. Sigrist, and M. B. Salamon, *Phys. Rev. Lett.* **97**, 017006 (2006).
- [6] M. Nishiyama, Y. Inada, and G.-q. Zheng, *Phys. Rev. Lett.* **98**, 047002 (2007).
- [7] G. M. Pang, M. Smidman, W. B. Jiang, J. K. Bao, Z. F. Weng, Y. F. Wang, L. Jiao, J. L. Zhang, G. H. Cao, and H. Q. Yuan, *Phys. Rev. B* **91**, 220502 (2015).
- [8] D. T. Adroja, A. Bhattacharyya, M. Telling, Y. Feng, M. Smidman, B. Pan, J. Zhao, A. D. Hillier, F. L. Pratt, and A. M. Strydom, *Phys. Rev. B* **92**, 134505 (2015).
- [9] J. Chen, L. Jiao, J. L. Zhang, Y. Chen, L. Yang, M. Nicklas, F. Steglich, and H. Q. Yuan, *New J. Phys.* **15**, 053005 (2013).
- [10] S. Kuroiwa, Y. Saura, J. Akimitsu, M. Hiraishi, M. Miyazaki, K. H. Satoh, S. Takeshita, and R. Kadono, *Phys. Rev. Lett.* **100**, 097002 (2008).
- [11] E. Bauer, G. Hilscher, H. Michor, C. Paul, E. W. Scheidt, A. Griбанov, Y. Seropegin, H. Noël, M. Sigrist, and P. Rogl, *Phys. Rev. Lett.* **92**, 027003 (2004).
- [12] E. M. Carnicom, W. w. Xie, T. Klimczuk, J. J. Lin, K. Górnicka, Z. Sobczak, N. P. Ong, and R. J. Cava, *Sci. Adv.* **4**, 7969 (2018).
- [13] A. D. Hillier, J. Quintanilla, and R. Cywinski, *Phys. Rev. Lett.* **102**, 117007 (2009).
- [14] J. A. T. Barker, D. Singh, A. Thamizhavel, A. D. Hillier, M. R. Lees, G. Balakrishnan, D. M. Paul, and R. P. Singh, *Phys. Rev. Lett.* **115**, 267001 (2015).
- [15] R. P. Singh, A. D. Hillier, B. Mazidian, J. Quintanilla, J. F. Annett, D. M. Paul, G. Balakrishnan, and M. R. Lees, *Phys. Rev. Lett.* **112**, 107002 (2014).
- [16] D. Singh, J. A. T. Barker, A. Thamizhavel, D. M. Paul, A. D. Hillier, and R. P. Singh, *Phys. Rev. B* **96**, 180501 (2017).
- [17] D. Singh, S. K. P. J. A. T. Barker, D. M. Paul, A. D. Hillier, and R. P. Singh, *Phys. Rev. B* **97**, 100505 (2018).
- [18] T. Shang, G. M. Pang, C. Baines, W. B. Jiang, W. Xie, A. Wang, M. Medarde, E. Pomjakushina, M. Shi, J. Mesot, H. Q. Yuan, and T. Shiroka, *Phys. Rev. B* **97**, 020502 (2018).
- [19] G. M. Luke, Y. Fudamoto, K. M. Kojima, M. I. Larkin, J. Mermin, B. Nachumi, Y. J. Uemura, Y. Maeno, Z. Q. Mao, Y. Mori, H. Nakamura, and M. Sigrist, *Nature* **394**, 558 (1998).
- [20] Y. Aoki, A. Tsuchiya, T. Kanayama, S. R. Saha, H. Sugawara, H. Sato, W. Higemoto, A. Koda, K. Ohishi, K. Nishiyama, and R. Kadono, *Phys. Rev. Lett.* **91**, 067003 (2003).
- [21] J. Xia, Y. Maeno, P. T. Beyersdorf, M. M. Fejer, and A. Kapitulnik, *Phys. Rev. Lett.* **97**, 167002 (2006).
- [22] E. R. Schemm, W. J. Gannon, C. M. Wishne, W. P. Halperin, and A. Kapitulnik, *Science* **345**, 190 (2014).
- [23] A. Sumiyama, D. Kawakatsu, J. Gouchi, A. Yamaguchi, G. Motoyama, Y. Hirose, R. Settai, and Y. Onuki, *J. Phys. Soc. Jpn.* **84**, 013702 (2014).
- [24] See the Supplemental Material at <http://link.aps.org/supplemental/xxx/PhysRevLett.xxxxx>, which includes Refs.[25-30].
- [25] N. R. Werthamer, E. Helfand, and P. C. Hohenberg, *Phys. Rev.* **147**, 295 (1966).
- [26] T. Klimczuk, Q. Xu, E. Morosan, J. D. Thompson, H. W. Zandbergen, and R. J. Cava, *Phys. Rev. B* **74**, 220502 (2006).
- [27] P. K. Biswas, M. R. Lees, A. D. Hillier, R. I. Smith, W. G. Marshall, and D. M. Paul, *Phys. Rev. B* **84**, 184529 (2011).
- [28] A. Tari, *The specific heat of matter at low temperatures* (Imperial College Press, London, 2003).
- [29] T. H. K. Barron and G. K. White, *Heat capacity and thermal expansion at low temperatures* (Kluwer, New York, 1999).
- [30] R. Waterstrat and R. Manuszewski, *J. Less-Common Met.* **51**, 55 (1977).
- [31] G. B. Balakrishnan, M. Smidman, A. D. Hillier, and D. M. Paul, “Rb1120180,” (2011), STFC ISIS Facility.
- [32] W. Barford and J. M. F. Gunn, *Physica C* **156**, 515 (1988).
- [33] E. H. Brandt, *Phys. Rev. B* **68**, 054506 (2003).
- [34] D. A. Mayoh, J. A. T. Barker, R. P. Singh, G. Balakrishnan, D. M. Paul, and M. R. Lees, *Phys. Rev. B* **96**, 064521 (2017).
- [35] D. Singh, A. D. Hillier, A. Thamizhavel, and R. P. Singh, *Phys. Rev. B* **96**, 064521 (2017).
- [36] B. Chen, Y. Guo, H. Wang, Q. Su, Q. Mao, J. Du, Y. Zhou, J. Yang, and M. Fang, *Phys. Rev. B* **94**, 024518 (2016).
- [37] J. Chen, L. Jiao, J. L. Zhang, Y. Chen, L. Yang, M. Nicklas, F. Steglich, and H. Q. Yuan, *Phys. Rev. B* **88**, 144510 (2013).
- [38] A. B. Karki, Y. M. Xiong, N. Haldolaarachchige, S. Stadler, I. Vekhter, P. W. Adams, D. P. Young, W. A. Phelan, and J. Y. Chan, *Phys. Rev. B* **83**, 144525 (2011).
- [39] C. Cirillo, R. Fittipaldi, M. Smidman, G. Carapella, C. Attanasio, A. Vecchione, R. P. Singh, M. R. Lees, G. Balakrishnan, and M. Cuoco, *Phys. Rev. B* **91**, 134508 (2015).
- [40] R. Kubo and T. Toyabe, *Magnetic Resonance and Relaxation*, edited by R. Blinc (North-Holland, Amsterdam, 1967).
- [41] A. Yaouanc and P. D. de Réotier, *Muon Spin Rotation, Relaxation, and Resonance: Applications to Condensed Matter* (Oxford University Press, Oxford, 2011).
- [42] P. K. Biswas, A. D. Hillier, M. R. Lees, and D. M. Paul, *Phys. Rev. B* **85**, 134505 (2012).
- [43] A. A. Aczel, T. J. Williams, T. Goko, J. P. Carlo, W. Yu, Y. J. Uemura, T. Klimczuk, J. D. Thompson, R. J. Cava, and G. M. Luke, *Phys. Rev. B* **82**, 024520 (2010).
- [44] D. Singh, J. A. T. Barker, T. Arumugam, A. D. Hillier, D. M. Paul, and R. P. Singh, *J. Phys. Condens. Matter* **30** (2018).
- [45] D. Singh, K. P. Sajilesh, S. Marik, A. D. Hillier, and R. P. Singh, *Supercond. Sci. Technol.* **30**, 125003 (2017).
- [46] J. Quintanilla, A. D. Hillier, J. F. Annett, and R. Cywinski, *Phys. Rev. B* **82**, 174511 (2010).
- [47] A. D. Hillier, J. Quintanilla, B. Mazidian, J. F. Annett, and R. Cywinski, *Phys. Rev. Lett.* **109**, 097001 (2012).
- [48] Z. F. Weng, J. L. Zhang, M. Smidman, T. Shang, J. Quintanilla, J. F. Annett, M. Nicklas, G. M. Pang, L. Jiao, W. B. Jiang, Y. Chen, F. Steglich, and H. Q. Yuan, *Phys. Rev. Lett.* **117**, 027001 (2016).
- [49] W.-C. Lee, S.-C. Zhang, and C. Wu, *Phys. Rev. Lett.* **102**, 217002 (2009).
- [50] S. Ghosh, J. F. Annett, and J. Quintanilla, *arXiv preprint arXiv:1803.02618v2* (2018).

[51] L. F. Mattheiss, [Phys. Rev. \*\*151\*\*, 450 \(1966\)](#).

## Supplementary material to Time-reversal symmetry breaking in Re superconductors

T. Shang,<sup>1,2,3</sup> M. Smidman,<sup>4</sup> S. K. Ghosh,<sup>5</sup> C. Baines,<sup>6</sup> L. J. Chang,<sup>7</sup> D. J. Gawryluk,<sup>1</sup> J. A. T. Barker,<sup>6</sup> R. P. Singh,<sup>8</sup> D. McK. Paul,<sup>9</sup> G. Balakrishnan,<sup>9</sup> E. Pomjakushina,<sup>1</sup> M. Shi,<sup>2</sup> M. Medarde,<sup>1</sup> A. D. Hillier,<sup>10</sup> H. Q. Yuan,<sup>4,11</sup> J. Quintanilla,<sup>5</sup> J. Mesot,<sup>12,3,13</sup> and T. Shiroka<sup>13,12</sup>

### Crystal structure

The purity and crystal structure of both  $\text{Re}_{0.82}\text{Nb}_{0.18}$  and pure Re were checked via x-ray powder diffraction (XRD). No impurity phases could be detected in either sample. As shown in Fig. S1(a), similarly to other  $\text{ReT}$  alloys, the XRD patterns of  $\text{Re}_{0.82}\text{Nb}_{0.18}$  can be well indexed by an  $\alpha$ -Mn-type noncentrosymmetric structure with space group  $I\bar{4}3m$  (217). On the other hand, as plotted in Fig. S1(b), the XRD of pure Re indicates a centrosymmetric hexagonal structure with space group  $P6_3/mmc$  (194). Both crystal structures are plotted in the insets. The derived lattice parameters for pure Re are  $a = b = 2.762 \text{ \AA}$ ,  $c = 4.457 \text{ \AA}$ , and for  $\text{Re}_{0.82}\text{Nb}_{0.18}$  are  $a = b = c = 9.636 \text{ \AA}$ , respectively. Table S1 summarizes the atomic coordinates of Re,  $\text{Re}_{0.82}\text{Nb}_{0.18}$ ,  $\text{Nb}_{0.5}\text{Os}_{0.5}$ , and  $\text{Mg}_{10}\text{Ir}_{19}\text{B}_{16}$ . Also  $\text{Nb}_{0.5}\text{Os}_{0.5}$  and  $\text{Mg}_{10}\text{Ir}_{19}\text{B}_{16}$  exhibit an  $\alpha$ -Mn-type noncentrosymmetric structure. Since the latter have the same noncentrosymmetric cubic space group as  $\text{ReT}$ , it is reasonable to expect a similar SOC-induced band splitting.

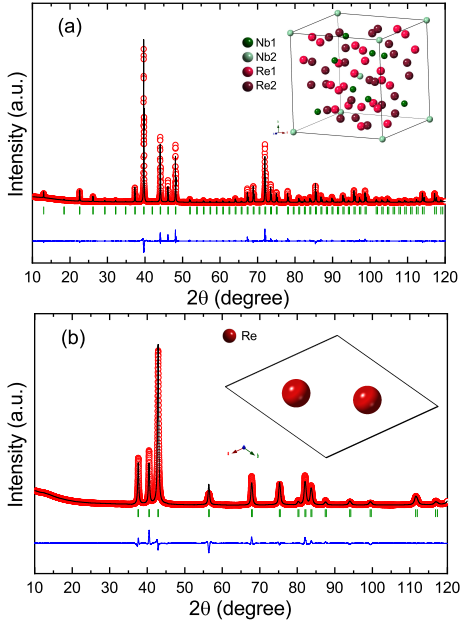


FIG. S1. Rietveld fits of the room-temperature x-ray powder diffraction patterns of  $\text{Re}_{0.82}\text{Nb}_{0.18}$  (a) and pure Re (b). Red circles show the experimental data, while black lines the refined profiles. Ticks below the patterns indicate the Bragg-peak reflections, while blue lines show the residues. Insets show the crystal structures.

### Upper critical field

As in the  $\text{Re}_{0.82}\text{Nb}_{0.18}$  case, also for pure Re we measured the field-dependent magnetization  $M(H)$  at various temperatures. As shown in Fig. S2,  $M(H)$  data between 1.9

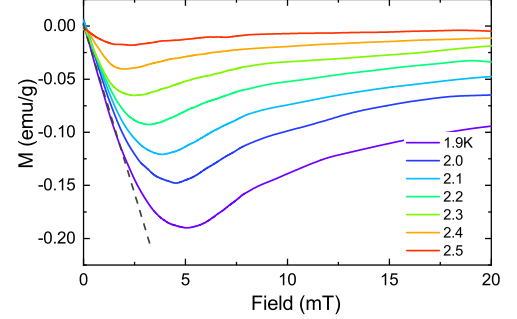


FIG. S2. Re magnetization vs. magnetic field recorded at different temperatures up to  $T_c$ . For each temperature,  $\mu_0 H_{c1}$  was determined from the  $M(H)$  deviation from linearity (dashed line).

and 2.5 K, display typical features of type-II superconductors. To calculate the penetration depth from  $\mu_0 H_{c1}$ , we investigated also the upper critical field  $\mu_0 H_{c2}$  of  $\text{Re}_{0.82}\text{Nb}_{0.18}$  by measuring its electrical resistivity  $\rho(T)$  and specific heat  $C(T)/T$  at various magnetic fields up to 9 T. As shown in Fig. S3(a) and (b), both  $\rho(T)$  and  $C(T)/T$  detect a zero-field superconducting transition temperature  $T_c(0) = 8.8 \text{ K}$ , decreasing with increasing field. The derived upper-critical-field  $\mu_0 H_{c2}(T)$  vs. normalized-temperature  $T/T_c$  data, summarized in Fig. S3(c), were further analyzed using the Werthamer-Helfand-Hohenberg (WHH) model [25]. The dash-dotted line in Fig. S3(c), refers to a WHH model with an orbital-limiting field only, which gives  $\mu_0 H_{c2}^{\text{WHH}}(0) = 15.6(1) \text{ T}$ . This is consistent with previously reported values [38] and very close to the weak-coupling Pauli paramagnetic limit  $[\mu_0 H_p = 1.86 T_c = 16.3(1) \text{ T}]$ .

In the Ginzburg-Landau theory of superconductivity, the magnetic penetration depth  $\lambda$  is related to the coherence length  $\xi$ , and the lower critical field via  $\mu_0 H_{c1} = (\Phi_0/4\pi\lambda^2)[\ln(\kappa) + \alpha(\kappa)]$ , where  $\Phi_0 = 2.07 \times 10^{-3} \text{ T } \mu\text{m}^2$  is the quantum of magnetic flux,  $\kappa = \lambda/\xi$  is the Ginzburg-Landau parameter, and  $\alpha(\kappa)$  is a parameter which converges to 0.497 for  $\kappa \gg 1$  [33]. By using  $\mu_0 H_{c1} = 6.4 \text{ mT}$  and  $\xi = 4.59 \text{ nm}$  (calculated from  $\mu_0 H_{c2}$ ) for  $\text{Re}_{0.82}\text{Nb}_{0.18}$ , the resulting  $\lambda_{\text{GL}} = 352(3) \text{ nm}$  is compatible with  $357(3) \text{ nm}$ , the experimental value from  $\mu\text{SR}$  data. The Ginzburg-Landau parameter  $\kappa \sim 59 \gg 1$  confirms once more that  $\text{Re}_{0.82}\text{Nb}_{0.18}$  is a strong type-II superconductor.

### Transverse-Field $\mu\text{SR}$

The optimal field value for TF- $\mu\text{SR}$  experiments was determined via preliminary field-dependent  $\mu\text{SR}$  depolarization-rate measurements at 1.5 K (see Fig. S4). The corresponding TF spectra are described by the same model [Eq. (1)] used in the main text. As shown in Fig. S4(c), the resulting Gaussian relaxation rate  $\sigma$  exhibits



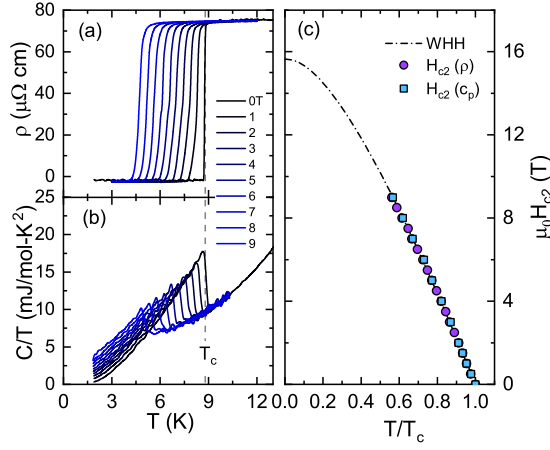


FIG. S3. Temperature dependence of the (a) electrical resistivity, and (b) specific heat, of  $\text{Re}_{0.82}\text{Nb}_{0.18}$  in various applied magnetic fields up to 9 T. (c) Upper critical field  $\mu_0 H_{c2}$  versus normalized temperature  $T/T_c$ . The dash-dotted line represents a fit to the WHH model taking into account only the orbital-limiting effect.

a maximum at 10 mT, close to the lower critical field value  $\mu_0 H_{c1}$ . By considering the decrease of intervortex distance with field and the vortex-core effects, a field of 15 mT was chosen for the temperature-dependent study at PSI, while the ISIS measurements were performed in a field of 30 mT.

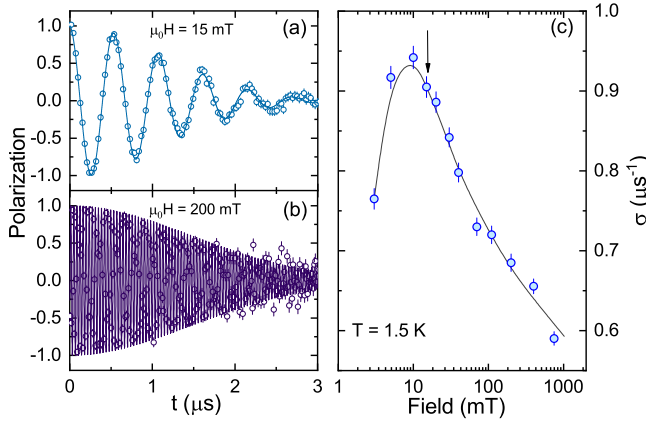


FIG. S4. Time-domain TF- $\mu$ SR spectra in the superconducting state of  $\text{Re}_{0.82}\text{Nb}_{0.18}$  measured at 15 mT (a) and 200 mT (b). The Gaussian relaxation rate vs. field exhibits a broad maximum near 10 mT (c). The arrow indicates the field value used in the  $T$ -dependent TF- $\mu$ SR measurements at PSI. The solid line is a guide to the eyes.

#### Zero-field specific heat

Figure S5 shows the temperature dependence of the total, electronic, and phononic specific heat of  $\text{Re}_{0.82}\text{Nb}_{0.18}$  measured below 15 K in zero field. To subtract the phonon contribution from the total specific heat, the normal-state specific heat is fitted to the expression  $C/T = \gamma_n + \beta T^2 + \delta T^4$ , where  $\gamma_n$  is the normal-state electronic specific-heat coefficient, whereas  $\beta$  and  $\delta$  are the phonon specific-heat coefficients [28, 29]. From the fit shown in the inset of Fig. S5 (dashed-line), the derived  $\gamma_n$ ,  $\beta$  and  $\delta$  values are  $4.4 \text{ mJ/mol-K}^2$ ,  $0.0582 \text{ mJ/mol-K}^4$  and  $0.00014 \text{ mJ/mol-K}^6$ . The phonon contribution can hence be calculated using

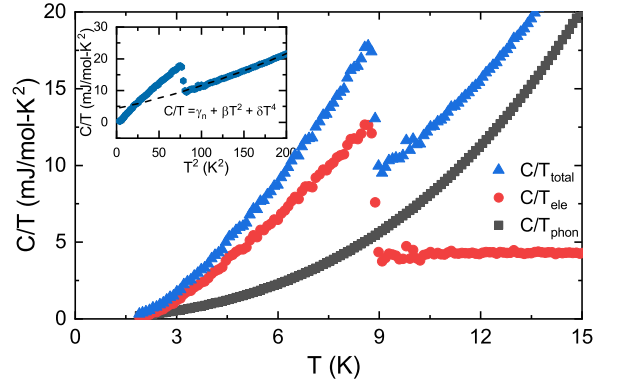


FIG. S5. Temperature dependence of the total, electronic, and phononic specific heat of  $\text{Re}_{0.82}\text{Nb}_{0.18}$  measured in zero field. The dashed-line in the inset is a fit to  $C/T = \gamma_n + \beta T^2 + \delta T^4$ .

Table S1. Atomic coordinates of Re,  $\text{Re}_{0.82}\text{Nb}_{0.18}$ ,  $\text{Nb}_{0.5}\text{Os}_{0.5}$ , and  $\text{Mg}_{10}\text{Ir}_{19}\text{B}_{16}$ . Data for the last two cases were taken from Refs. 26, 30, and 44.

Re ( $P6_3/mmc$ ; $a = b = 2.762 \text{ \AA}$ , $c = 4.457 \text{ \AA}$ )				
Atom	Wyckoff position	$x$	$y$	$z$
Re	2c	0.33330	0.66670	0.25000
$\text{Re}_{0.82}\text{Nb}_{0.18}$ ( $I\bar{4}3m$ ; $a = b = c = 9.636 \text{ \AA}$ )				
Atom	Wyckoff position	$x$	$y$	$z$
Nb <sub>1</sub>	2a	0	0	0
Nb <sub>2</sub>	8c	0.3179	0.3179	0.3179
Re <sub>1</sub>	24g	0.3592	0.3592	0.0413
Re <sub>2</sub>	24g	0.0912	0.0912	0.2842
$\text{Nb}_{0.5}\text{Os}_{0.5}$ ( $I\bar{4}3m$ ; $a = b = c = 9.765 \text{ \AA}$ )				
Atom	Wyckoff position	$x$	$y$	$z$
Nb <sub>1</sub>	2a	0	0	0
Os <sub>1</sub>	2c	0	0	0
Nb <sub>2</sub>	8c	0.3170	0.3170	0.3170
Os <sub>2</sub>	8c	0.3170	0.3170	0.3170
Nb <sub>3</sub>	24g	0.3560	0.3560	0.0420
Os <sub>3</sub>	24g	0.3560	0.3560	0.0420
Nb <sub>4</sub>	24g	0.0809	0.0809	0.2780
Os <sub>4</sub>	24g	0.0809	0.0809	0.2780
$\text{Mg}_{10}\text{Ir}_{19}\text{B}_{16}$ ( $I\bar{4}3m$ ; $a = b = c = 10.568 \text{ \AA}$ )				
Atom	Wyckoff position	$x$	$y$	$z$
Ir <sub>1</sub>	2a	0	0	0
Ir <sub>2</sub>	12d	0	0.25	0.5
Ir <sub>3</sub>	24g	0.0703	0.2525	0.2525
Mg <sub>1</sub>	8c	0.3331	0.3331	0.3331
Mg <sub>2</sub>	12e	0	0	0.3473
B <sub>1</sub>	8c	0.1127	0.1127	0.1127
B <sub>2</sub>	24g	0.1639	0.1639	0.4140

the expression,  $C/T_{\text{phon}} = \beta T^2 + \delta T^4$ , which is then subtracted from the experimental data. The resulting  $C/T_{\text{ele}} = C/T_{\text{total}} - C/T_{\text{phon}}$  curve (shown with red symbols in Fig. S5), represents the electronic specific heat.



Table SII. Nuclear moment (in nuclear magnetons  $\mu_N$ ), muon-spin relaxation (at base temperature), calculated internal field, and superconducting parameters for  $\alpha$ -Mn-type  $\text{ReT}$ -NCSC and the pure Re metal. The internal field is calculated using  $B_{\text{int}} = \sqrt{2}\sigma_{\text{int}}/\gamma_\mu$ , where  $\sigma_{\text{int}}$  represents the change of muon relaxation rate between the normal and superconducting states. Except for  $\text{Re}_3\text{W}$ , where  $\sigma_{\text{int}}$  is expected to be below the resolution of the  $\mu\text{SR}$  technique, all the listed materials show spontaneous magnetic fields below  $T_c$ .

$\text{ReT}$	$M(\mu_N)$	$\sigma(\mu\text{s}^{-1})$	$\Lambda(\mu\text{s}^{-1})$	$B_{\text{int}}(\mu\text{T})$	$T_c(\text{K})$	$\mu_0 H_{c1}(\text{mT})$	$\mu_0 H_{c2}(\text{T})$	$\xi_{\text{GL}}(\text{\AA})$	$\lambda_{\text{GL}}(\text{\AA})$	$\kappa_{\text{GL}}$	$\lambda_{\text{eff}}(\text{\AA})$	$\Delta_0(\text{meV})$	$\Delta C/\gamma T_c$
$\text{Re}_3\text{W}$ [27, 42]	2.778	0.266	—	0.0	7.80	9.7	12.5	51.3	2571	50.0	4180	1.38	1.50
$\text{Re}_{24}\text{Ti}_5$ [18]	2.943	0.256	0.017	9.0	6.00	8.3	11.2	54.1	2860	53.0	3921	1.08	1.40
$\text{Re}_6\text{Ti}$ [17]	2.990	0.251	0.027	14.0	6.00	5.8	11.5	53.5	3490	65.2	4937	0.95	1.58
$\text{Re}_6\text{Zr}$ [15, 34]	3.010	0.264	0.022	11.0	6.75	8.0	11.6	53.3	3696	69.3	3086	1.21	1.60
$\text{Re}_6\text{Hf}$ [16, 35, 36]	2.970	0.262	0.035	8.5	5.96	5.6	12.2	52.0	3538	69.0	4620	1.10	1.53
$\text{Re}_{0.82}\text{Nb}_{0.18}$	3.910	0.392	0.007	38.2	8.8	6.4	15.6	45.9	3528	59.0	3567	1.61	1.94
Re	3.207	0.326	0.003	17.5	2.7	3.7	—	—	—	—	—	—	—

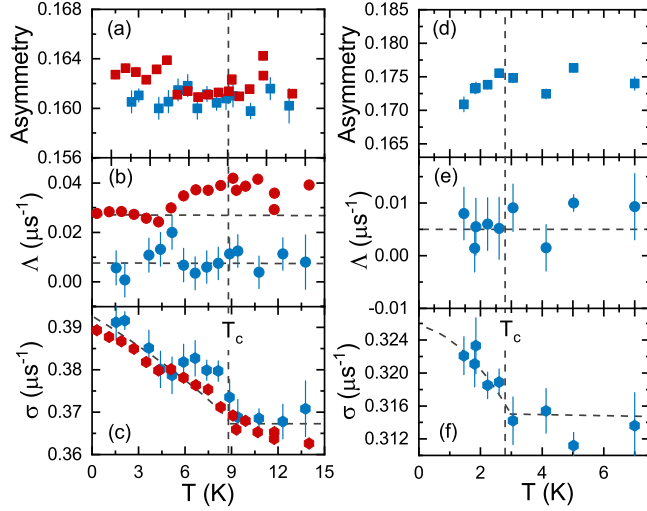


FIG. S6. ZF- $\mu\text{SR}$  fit parameters vs. temperature for  $\text{Re}_{0.82}\text{Nb}_{0.18}$  (a)-(c) and pure Re (d)-(f). Blue symbols represent datasets collected at PSI, while red symbols refer to datasets collected at ISIS. For comparison, the asymmetry of data collected at ISIS was divided by a factor of 1.25. The dashed lines are guide to the eyes.

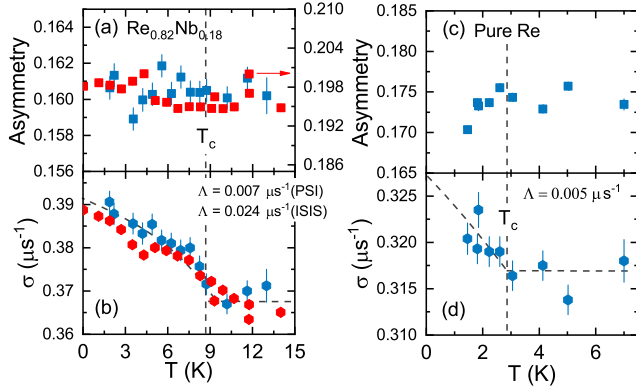


FIG. S7. ZF- $\mu\text{SR}$  fit parameters vs. temperature for  $\text{Re}_{0.82}\text{Nb}_{0.18}$  (a)-(b) and pure Re (c)-(d). The reported  $\Lambda$  value for  $\text{Re}_{0.82}\text{Nb}_{0.18}$  is the average of 0.007 (PSI) and 0.024 (ISIS), while for Re it is  $0.005 \mu\text{s}^{-1}$ . The blue symbols refer to datasets collected at PSI, while the red symbols to datasets collected at ISIS. The dashed lines are guide to the eyes.

### Zero-field $\mu\text{SR}$

The ZF- $\mu\text{SR}$  data were analyzed by combined Lorentzian and Gaussian Kubo-Toyabe relaxation function [see details

in Eq. (3) in the main text]. The polarization parameters  $P_s$  and  $P_{\text{bg}}$  were obtained by dividing the time-dependent asymmetry  $A(t)$  by its initial value  $A_0$ . The initial asymmetry parameter  $A_0$  was allowed to change with temperature, while the background signal was fixed for all the temperatures since, considering the limited temperature range of the measurements, we do not expect an appreciable change in background. The initial asymmetry of the background signal  $A_{\text{bg}}$  ( $P_{\text{bg}} = A_{\text{bg}}/A_0$ ) was determined by fits to data at base temperature and then fixed for all the temperatures. It is close to 3% of total asymmetry  $A_0$  in  $\text{Re}_{0.82}\text{Nb}_{0.18}$  (PSI) and to 2% in pure Re. The reduced total asymmetry for datasets collected at PSI [see Fig. S6(a)] reflects ZF-measurements carried out in transverse mode, i.e., with the initial muon-spin perpendicular to muon momentum, implying a loss of one third of the asymmetry. From Fig. S6, only the Gaussian muon-relaxation rate  $\sigma(T)$  exhibits a small but distinct increase below  $T_c$ , while the other parameters show a weak temperature dependence with no clear anomaly across  $T_c$ . In case of pure Re powders, the data in the inset of Fig. 3(b) of the main text were fitted with a fixed  $\Lambda$  value of  $0.003 \mu\text{s}^{-1}$ . Here we re-analyze the ZF- $\mu\text{SR}$  data on Re powders by releasing  $\Lambda$ . The derived parameters are summarized in Figs. S6 (d)-(f); again only  $\sigma(T)$  exhibits clear anomaly below  $T_c$ .

To confirm the above conclusions, all ZF- $\mu\text{SR}$  data were re-analyzed by fixing  $\Lambda$ s to the respective average values, as estimated from preliminary analyses with freely varying  $\Lambda$  values (see Fig. S6). As shown by dashed lines in panels (b) and (e), the average  $\Lambda$  values turned out to be  $0.007$  (PSI)/ $0.024$  (ISIS) and  $0.005 \mu\text{s}^{-1}$  for  $\text{Re}_{0.82}\text{Nb}_{0.18}$  and pure Re, respectively. In both cases, the derived parameters, including the asymmetry and muon-spin relaxation rate  $\sigma$ , are shown in Fig. S7. Clearly, the evolution of  $\sigma$  with temperature remains robust in both compounds, hence implying that the spontaneous magnetic fields we detect via ZF- $\mu\text{SR}$  are an *intrinsic effect* and not a fit artifact. This is further confirmed in Fig. S8, where we show the cross correlations between the different fit parameters. The lack of any visible trends (i.e., the lack of correlations) confirms once more the *intrinsic nature of TRSB* in both pure Re and  $\text{Re}_{0.82}\text{Nb}_{0.18}$ .

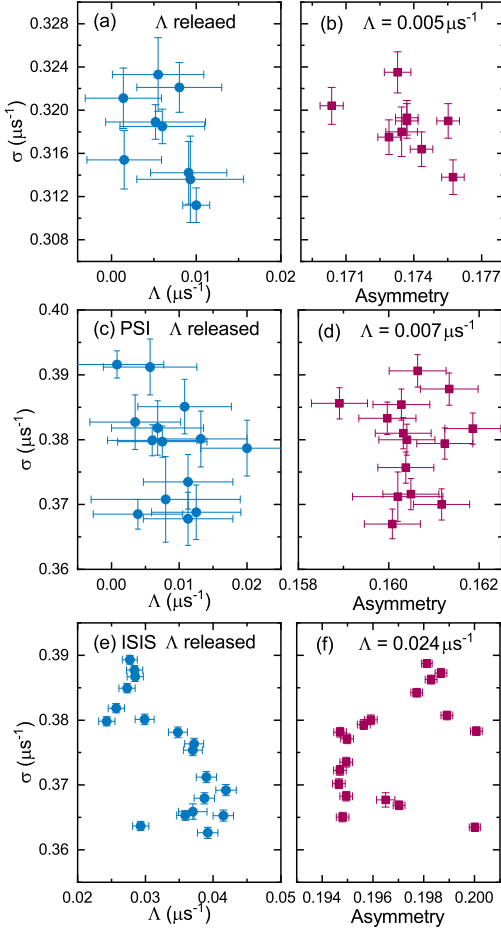


FIG. S8. Cross correlations of ZF- $\mu$ SR fit parameters for pure Re (a)-(b) and  $\text{Re}_{0.82}\text{Nb}_{0.18}$  (c)-(f). The vertical axis shows  $\sigma$ , while the horizontal axis  $\Lambda$  or asymmetry. In both cases, the rather random distribution of points indicates a lack of any relevant correlations between the fit parameters.

### Symmetry analysis

In this section we provide further details on the symmetry-allowed TRS-breaking order parameter in  $\text{Re}_{0.82}\text{Nb}_{0.18}$  and in pure Re.

#### $\text{Re}_{0.82}\text{Nb}_{0.18}$

The  $\text{Re}_{0.82}\text{Nb}_{0.18}$  system has the same non-centrosymmetric *bcc* crystal structure as other  $\text{Re}_6$  (Zr, Hf, Ti) materials with a symmorphic space group  $I43m$  and corresponding point group  $T_d$ . A standard symmetry analysis [15] finds that both the 2D irreducible representation (irrep) and the two 3D irreps of  $T_d$  support TRS breaking instabilities. Assuming strong SOC and writing the pair potential as  $\hat{\Delta}(\vec{k}) = i[\Delta_0(\vec{k}) + \vec{d}(\vec{k}) \cdot \hat{\sigma}] \hat{\sigma}_y$ , the TRS breaking instability for the 2D irrep corresponds to [15]:

$$\Delta_0(\vec{k}) = (2k_z^2 - k_x^2 - k_y^2) + i(k_x^2 - k_y^2),$$

$$\vec{d}(\vec{k}) = [k_x(k_y^2 - k_z^2), k_y(k_x^2 - k_z^2), k_z(k_x^2 - k_y^2)] \Delta_0(\vec{k}).$$

This leads to a vanishing pair potential at eight symmetry-required point nodes, given by  $\phi = \pm\pi/4, \pm 3\pi/4$  and  $\theta =$

Table SIII. Basis functions of  $D_3$ .

$D_3$	Basis functions	
Irreps	Scalar (even)	Vector (odd)
$A_1$	$[A + B(k_x^2 + k_y^2) + Ck_z^2]$	$[A(k_x\hat{x} + k_y\hat{y}) + Bk_z\hat{z}]$
$A_2$	$Ak_zk_x(k_x^2 - 3k_y^2)$	$Ak_y(k_y^2 - 3k_x^2)\hat{z}$
$E$	$Ak_z \begin{pmatrix} k_x \\ k_y \end{pmatrix}$	$\begin{pmatrix} Ak_z\hat{x} + Bk_x\hat{z} \\ Ak_z\hat{y} + Bk_y\hat{z} \end{pmatrix}$

$\arctan(\sqrt{2}), \pi - \arctan(\sqrt{2})$ , as shown in Fig. S9(a) and S9(d).

Similarly, for the two 3D irreps,  $F_1$  and  $F_2$ , the TRS breaking pair potentials are, respectively [15]:

$$\Delta_0(\vec{k}) = k_z(k_y + ik_x)(k_x^2 - k_y^2)(k_y^2 - k_z^2)(k_z^2 - k_x^2),$$

$$\vec{d}(\vec{k}) = (1, i, 0)k_xk_yk_z$$

and

$$\Delta_0(\vec{k}) = (k_y + ik_x)k_z,$$

$$\vec{d}(\vec{k}) = (1, i, 0)k_xk_yk_z(k_x^2 - k_y^2)(k_y^2 - k_z^2)(k_z^2 - k_x^2).$$

In both cases, the pair potential vanishes at the ‘North’ and ‘South’ poles,  $\theta = 0$  and  $\pi$ , and at the line nodes at the ‘equator’,  $\theta = \pi/2$ , as shown in Fig. S9(b) and S9(e) for the  $F_1$  case and in Fig. S9(c) and S9(f) for the  $F_2$  case.

#### Pure Re

Re has a hexagonal structure with nonsymmorphic space group  $P6_3/mmc$  (No. 194 – point group  $D_{6h}$ ) with two atoms per unit cell. Due to its centrosymmetric nature, this space group has separate singlet and triplet uniform superconducting instabilities. They are given by the symmetries of the factor group  $\mathcal{G}_{194} = \{P6_3/mmc\}/\mathcal{T}$  ( $\mathcal{T}$  is the group of pure primitive translations), which is isomorphic to  $D_{6h}$ . Hence,  $\mathcal{G}_{194}$  has the 2D irreps  $E_g$  and  $E_u$  which, in principle, allow the TRS breaking of the order parameter by a non-trivial phase difference between the two components of a possible two-component order parameter. In general, compared to a symmorphic crystal, finding the possible forms of the gap function is complicated by the fact that the basis functions of the point group  $D_{6h}$  cannot simply be used as building blocks of the pairing potential. Nevertheless, it is straightforward to enumerate the pairing potentials that do not break glide-plane or screw-axis symmetries. These correspond to the  $D_{3d}$  subgroup of  $\mathcal{G}_{194}$ , containing only its symmorphic symmetries. We note that  $D_{3d} = D_3 \otimes i$ , which is the group of symmetries of an equilateral triangle. The simplest basis functions of  $D_3$  are given in Table SIII. Clearly,  $D_3$  does include a 2D irrep and thus allows for TRS breaking both in the singlet- ( $E_g$  irrep of  $D_{3d}$ ) or in the triplet channel ( $E_u$  irrep of  $D_{3d}$ ).

In this case, to compute the possible singlet ground states, we write the most general form of the order parameter just below  $T_c$ , compatible with the relevant basis functions:

$$\Delta_0(\mathbf{k}) = (\eta_1 k_x k_x + \eta_2 k_z k_y) \quad (1)$$

and then obtain a general expression of the free energy, expressed as a function of the two pairing components  $\eta_1, \eta_2$ ,

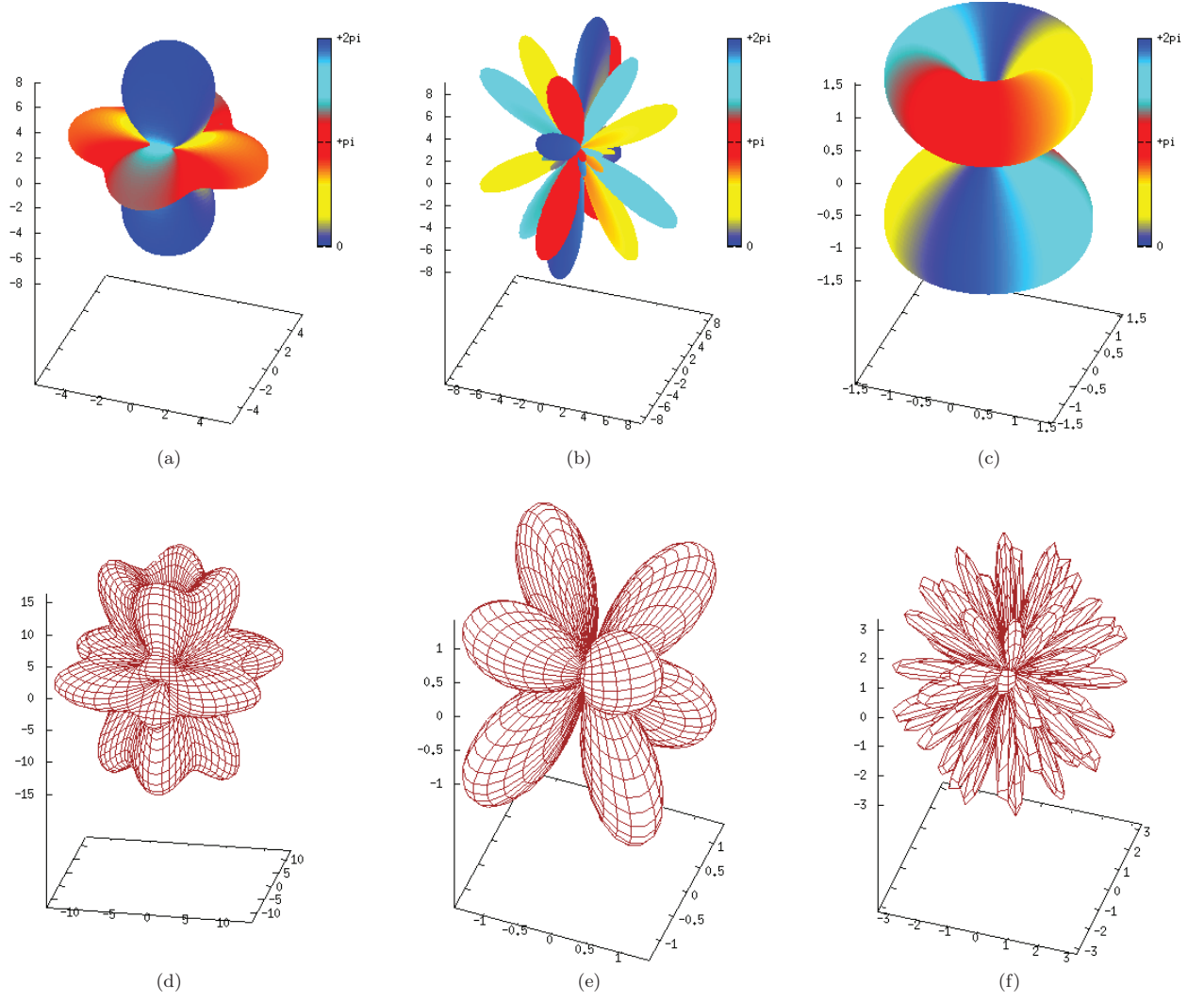


FIG. S9. Polar plot of the symmetry-allowed TRSB order parameters in  $\text{Re}_6\text{T}$ , for the  $E$ ,  $F_1$ , and  $F_2$  irreps, respectively. Panels (a), (b), and (c) depict the *magnitude* of the *singlet* part of the order parameter, with the corresponding *phase* shown in color. Panels (d), (e), and (f) instead show the magnitude of the *triplet* order parameter  $\vec{d}(\vec{k})$  for the three cases, respectively.

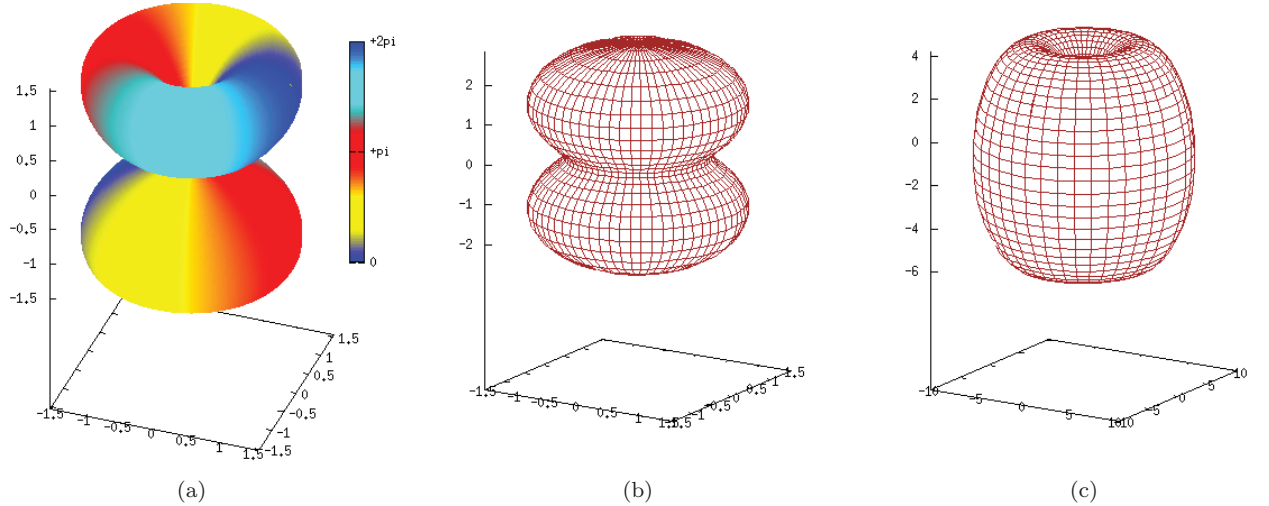


FIG. S10. Polar plot of the TRSB order parameters of pure  $\text{Re}$  corresponding to the  $D_{3d}$  subgroup (taking  $A = 1/2$  and  $B = 1/3$ ). (a) The *magnitude* of the *singlet* TRSB order parameter with the corresponding *phase* shown in color. (b) The magnitude of  $\vec{d}(\vec{k})$  corresponding to the *triplet* TRSB order parameter. (c) The lowest excitation gap at the Fermi energy for the triplet TRSB order parameter given in Eq. (S4).

by requiring that it respects the symmetries of  $D_{3d}$ :

$$\mathcal{F} = a(|\eta_1|^2 + |\eta_2|^2) + \beta_1(|\eta_1|^2 + |\eta_2|^2)^2 + \beta_2(\eta_1^* \eta_2 - \eta_1 \eta_2^*)^2 + \dots$$

Minimization of this quartic polynomial gives two stable ground states:  $(\eta_1, \eta_2) = (1, 0)$  and  $(1, i)$ . The latter is the

only one that breaks TRS and it gives

$$\Delta_0(\vec{k}) = Ak_z(k_x + ik_y). \quad (2)$$

This corresponds to a singlet energy gap  $|A||k_z|\sqrt{k_x^2 + k_y^2}$ . The low-energy excitations would thus be dominated by a line node at the ‘equator’,  $\theta = \pi/2$ , and point nodes at  $\theta = 0, \pi$ , as shown in Fig. S10(a).

A similar procedure applied to the triplet channel gives one TRS breaking state with a  $d$ -vector:

$$\vec{d}(\vec{k}) = [Ak_z, iAk_z, B(k_x + ik_y)]. \quad (3)$$

The variation of its magnitude is shown in Fig. S10(b). The corresponding lowest excitation energy gap is given by:

$$\Delta_{\min} = \sqrt{g(k_x, k_y) + 2A^2k_z^2 - 2|A|k_z\sqrt{g(k_x, k_y) + A^2k_z^2}} \quad (4)$$

where  $g(k_x, k_y) = B^2(k_x^2 + k_y^2)$ . As shown in Fig. S10(c), it has two point nodes at the ‘poles’,  $\theta = 0, \pi$ , but no line nodes.